Research Square

Preprints are preliminary reports that have not undergone peer review.
They should not be considered conclusive, used to inform clinical practice,
or referenced by the media as validated information.

Technogenic nature of radionuclide distribution at operating uranium sorption sites in Uzbekistan: a comprehensive assessment of air, surface, and soil compartments

Umidjon Haydarov

xaydarovumid02@gmail.com

Samarkand State University named after Sharof Rashidov

Amrullo Muzafarov

Navoi State Mining and Technological University

Alisher Jurakulov

Navoi State Mining and Technological University

Dilfuza Sidiqova

Navoi State Mining and Technological University

Diyor Khazratov

Samarkand State University named after Sharof Rashidov

Research Article

Keywords: Radon progeny, Uranium in-situ leaching, Occupational radiation protection, Surface alpha contamination, Radiation hazard indices, Spearman correlation

Posted Date: September 23rd, 2026

DOI: https://doi.org/10.21203/rs.3.rs-10599042/v1

License: This work is licensed under a Creative Commons Attribution 4.0 International License.
Read Full License

Additional Declarations: No competing interests reported.

Technogenic nature of radionuclide distribution at operating uranium sorption sites in Uzbekistan: a comprehensive assessment of air, surface, and soil compartments

Umidjon Haydarov[1*], Amrullo Muzafarov[2], Alisher Jurakulov[2], Dilfuza Sidiqova[2], Diyor Khazratov[1]

[1]Institute of Nuclear Technologies, Samarkand State University named after Sharof Rashidov, Samarkand 140104, Uzbekistan

[2]Navoi State Mining and Technological University, Navoi 210100, Uzbekistan

Email addresses:

Umidjon Haydarov*: xaydarovumid02@gmail.com; ORCID: https://orcid.org/0009-0007-1845-3277

Amrullo Muzafarov: a.muzafarov@ngmk.uz

Alisher Jurakulov: ali_80_84@mail.ru

Dilfuza Sidiqova: dilfuzasidiqova01@gmail.com

Diyor Khazratov: diyorxazratov32@gmail.com

*Corresponding author: xaydarovumid02@gmail.com

Abstract At operating uranium sorption sites (USS), radon, airborne aerosols, external gamma radiation, surface contamination, and soil radionuclides coexist, forming a complex radiation environment. However, their interrelationships and connection to the technological process remain poorly studied under conditions of active uranium production. This study assessed the radiation situation at six USS in Uzbekistan to determine whether elevated radiation indicators reflect the natural geological background or the technological process. At eight functional zones of each USS and eight control points, the equilibrium equivalent radon concentration (EERC), long-lived alpha-active aerosols (LLAA), ambient dose equivalent rate H*(10), surface alpha contamination, and soil activities of ^{40}K, ^{226}Ra, and ^{232}Th were measured, and radiation hazard indices were calculated. At the resin exchange platform and sorption columns, EERC was 3.8–4.3 times higher than at control points, LLAA was nearly 3 times higher ($p < 0.001$), H*(10) reached 5.6-fold above background, and surface alpha contamination reached 3.5 times the IAEA criterion (0.4 Bq cm^{-2}). In contrast, soil radionuclide activities and all radiation hazard indices remained below internationally recommended limits. Although the USS-control difference was statistically significant, it was practically small (≈18%). Strong correlations among the radiation indicators ($\rho = 0.477–0.916$) and their consistently elevated levels in the same functional zones confirmed that uranium sorption operations are the principal source of the observed radiation anomalies.

Keywords Radon progeny; Uranium in-situ leaching; Occupational radiation protection; Surface alpha contamination; Radiation hazard indices; Spearman correlation

Introduction

In recent decades, the rapid development of nuclear power and the expansion of the nuclear fuel cycle have driven a steady increase in the demand for uranium feedstock (OECD NEA & IAEA 2025). Uzbekistan, one of the countries with major uranium resources, also carries out most of its uranium mining using this technology (IAEA 1997; Navoiyuran 2026a; WNA 2026). Although in-situ leaching (ISL) is distinguished by its high efficiency and relatively low surface disturbance, direct handling of uranium-bearing solutions creates conditions for radon emission, the formation of radioactive aerosols, and the dispersion of radionuclides into environmental compartments (IAEA 2005; Li and Yao 2024).

In uranium-industry areas, the radiation environment is shaped primarily by radionuclides of the uranium decay series together with the natural isotopes ^{232}Th and ^{40}K. These radionuclides occur in soil, atmospheric air, and water, where they constitute the principal natural sources of external gamma radiation and internal exposure (UNSCEAR 2010). Radon (^{222}Rn), a natural radioactive noble gas belonging to the ^{238}U decay chain, is one of the main sources of natural radiation in atmospheric air. Owing to its relatively long half-life (3.82 days), it can escape from soil and rocks into the atmosphere and accumulate in enclosed buildings and at uranium-industry facilities. In addition, the short- and long-lived decay products formed by ^{222}Rn decay are important indicators in assessing the radiation risk to workers and to the population living in nearby areas (IAEA 2020; Kreuzer and McLaughlin 2010; UNSCEAR 2010). The environmental distribution of these radionuclides depends simultaneously on the geological structure, climatic factors, wind regime, and the intensity of anthropogenic activity. Therefore, identifying the source of the elevated levels observed in uranium production areas, separating the contributions of the natural geological background and the technological impact-becomes a central methodological task of radiation assessment (IAEA 2005; UNSCEAR 2010).

According to IAEA data, the occupational exposure of workers at uranium ore processing facilities is formed mainly through three exposure pathways: external gamma radiation (44%), inhalation of long-lived radioactive dust (LLRD) (34%), and inhalation of radon decay products (RDP) (22%) (IAEA 2020). These data show that the radiation risk is formed not by a single factor but by the combination of several exposure pathways.

In addition to airborne radiation indicators, the surface alpha contamination of production surfaces and technological equipment is also one of the important indicators for radiation safety assessment. Surface contamination reflects the accumulation of uranium-decay-series radionuclides on technological equipment and working surfaces and may increase the internal exposure risk to workers through the inhalation or accidental ingestion of radioactive particles. Therefore, a reliable assessment of the radiation situation at uranium production facilities requires not a single component but an integrated analysis of atmospheric air, external gamma background, working surfaces, and soil indicators in their interrelation (IAEA 2005, 2020; Sasano et al. 2025).

In recent years, studies of the radiation situation in uranium mining areas have been carried out in various countries; most of them have been limited to former uranium mines, waste storage facilities, or the assessment of individual components of the radiological environment (Bakhtin et al. 2025; Egemberdieva et al. 2025; Kashkinbayev et al. 2025; Lesbek et al. 2025; Lespukh et al. 2013; Liu et al. 2021; Pandit et al. 2020). A recently published review likewise notes that the main body of ISL research has focused on groundwater and hydrogeochemistry, whereas radiological studies of atmospheric air, soil, and the working environment remain insufficiently developed (Mussayeva et al. 2026). Work carried out in Uzbekistan has mainly focused on radioactive waste storage facilities (Haydarov et al. 2026; Stegnar et al. 2013; Tsukatani et al. 2008) or on natural areas (Khasanov et al. 2024; Safarov et al. 2023; Tukhtaev et al. 2024). Although earlier radioecological assessments at uranium production facilities covered a broad range of radiation factors, they were mainly descriptive and based on comparison with regulatory values (Allaberganova et al. 2023; Kholov et al. 2021; Muzafarov et al. 2016; Urunov et al. 2024). In those studies, no analysis by functional zone was carried out, and the relationships among radiological indicators were not evaluated using statistical methods. Thus, studies that jointly assess radiation indicators across functional zones at active ISL sorption sites and statistically analyze their interrelationships are still limited.

For this purpose, the present study aims to compare the radiation indicators at operating uranium sorption sites (USS) with those at control points and to assess the origin of the observed differences. The study hypothesis is that the systematically elevated radiological indicators in certain functional zones, together with the practically small difference in natural-radionuclide activity in soil between the USS and control groups, indicate that the observed radiation situation is associated mainly with the technological process.

To achieve the stated aim, the study encompasses the following objectives:

(1) to assess the equilibrium equivalent radon concentration (EERC) and the concentration of long-lived alpha-active aerosols (LLAA) in atmospheric air;

(2) to assess the ambient dose equivalent rate H*(10) at the technogenic objects and control points;

(3) to determine the surface alpha contamination on the surfaces of the technogenic objects;

(4) to determine the activity concentrations of the radionuclides ^{226}Ra, ^{232}Th, and ^{40}K in soil and the associated radiation hazard indices;

(5) to assess, using non-parametric statistical tests and correlation analysis, the differences among functional zones and between groups, and the relationships among indicators;

(6) to discuss, based on all indicators, the dispersion characteristics of radionuclides from technogenic sources.

Unlike a descriptive assessment of individual radiological indicators, this study analyzes atmospheric air, external gamma radiation, surface alpha contamination, and soil radionuclides across functional zones and examines their

interrelationships using statistical methods. Such an approach makes it possible to assess the association of the radiation indicators with a technogenic source and their spatial distribution characteristics. The results serve to improve source-oriented radiation protection measures at operating sorption facilities and to provide a scientific basis for decisions aimed at ensuring the radiation safety of workers and of the population in nearby areas.

Study area and sampling sites

The study was carried out at USS located in the Samarkand region of Uzbekistan and in the nearby residential areas. The climate of this region is arid continental, with relatively cold winters and hot, dry summers. The annual precipitation is approximately 380 mm. The mean temperature in January ranges from −0.9 to +1.9 °C, while in summer the maximum temperature recorded was +40 to +44 °C (Gulomov and Vahobov 2017; World Bank Group 2020). Geologically, the area belongs to the south-eastern part of the Central Kyzylkum region – the zone of sandstone roll-front-type uranium deposits (Ibragimov 2016). These deposits are associated with hydrogenous sandstone sediments, and since 1994 uranium mining has been carried out mainly by the ISL method (Navoiyuran 2026b; WNA 2026). The study was conducted at six sorption sites (USS-1–USS-6) of an operating uranium ISL complex. The sites are located within an area of approximately 11 × 15 km, and samples were collected at each site. Measurements were made in eight functional zones: the general site area (Site area), pressurized sorption columns No. 1 and No. 2 (SC1, SC2), the resin exchange platform (REP), the water reservoir (WR), the pump station (PST), the operator room (OPR), and the canteen (CAN). To assess the migration of radionuclides from the technogenic source into the environment, sampling and measurements were also carried out at eight control points (CP1–CP8) located in nearby settlements at distances of 0.95–4.5 km (mean ≈ 2.5 km) from the sites. More control points were established in the more densely populated eastern and north-eastern zone, and fewer in the sparsely populated western part.

The relative locations of the sites and control points are shown in Fig. 1. Because the facility is a strategic uranium production installation, the exact geographic coordinates of the sites and control points and the names of the settlements are not disclosed, in accordance with the enterprise's internal regime and information-security requirements.

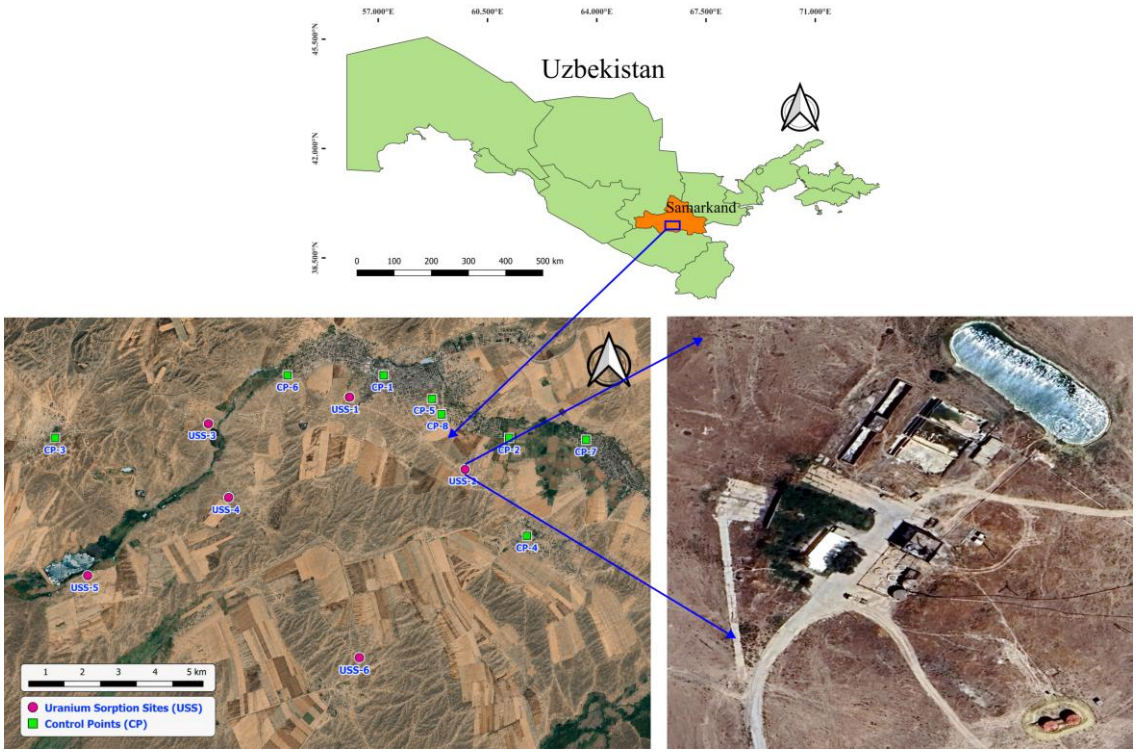

Fig. 1 Location of the six uranium sorption sites (USS-1–USS-6) and eight control points (CP-1–CP-8) in the Samarkand region, Uzbekistan. The right panel shows a close-up view of a representative site (USS-2).

The measurement and sampling points for the various radiation indicators differed depending on the nature of the study object. This distribution is presented in Table 1.

Table 1 Types of radiological measurements and the points at which they were carried out.

Measurement	**Uranium sorption sites (6 USS × 8 functional zones)**	**Control points (8 CP)**
EERC (Bq m^{-3})	Site area, SC1, SC2, REP, WR, PST, OPR, CAN	CP-1–CP-8
LLAA (mBq m^{-3})	Site area, SC1, SC2, REP, WR, PST, OPR, CAN	CP-1–CP-8
H*(10) (μSv h^{-1})	Site area, SC1, SC2, REP, WR, PST, OPR, CAN	CP-1–CP-8
Surface alpha contamination (Bq cm^{-2})	SC1, SC2, REP, PST, OPR, CAN	Not measured
Soil radionuclides (Bq kg^{-1})	Site area	CP-1–CP-8

Surface alpha contamination was measured only on the hard surfaces of the technological equipment and production rooms. Because the general site area (Site area) and the water reservoir (WR) have no technological contact surface, and because the control points are located outside the technological process, surface alpha contamination was not measured in these zones. Soil samples were taken from the general site area of each site and control point; sampling in the inner zones where the technological equipment is located was not possible.

Materials and methods

Determination of the equilibrium equivalent radon concentration (EERC)

The EERC in indoor and outdoor air was determined using an Alpharad Plus-AR automated compact radiometric complex (NTM-Zashchita Ltd. 2012). This modification combines the EERC and radon volumetric activity measurement units in a single housing and allows radon and thoron decay products to be recorded from the air by aspiration. The measurement is based on the principle of collecting the dispersed phase of radioactive aerosols on an aerosol filter and recording the alpha particles emitted by the radon and thoron decay products (^{218}Po, ^{214}Po, and others) accumulated on the filter. The airflow through the filter is 10 L min^{-1}. The instrument's EERC measurement range is 1.0 – 1.0 × 10^{6} Bq m^{-3}, and the main relative error is ±30%.

Indoor measurements were carried out in the operator and canteen rooms of the USS and, in residential areas, mainly in bedrooms and guest rooms. Windows and doors were kept closed for at least 30 minutes before and during the measurements. The instrument was placed at breathing height (approximately 1–1.5 m above the floor), at least 50 cm from walls and at least 1 m from ventilation sources (Puchkov et al. 2022).

Outdoor measurements were carried out under the natural conditions of the atmospheric air. The instrument was mounted approximately 1–1.5 m above ground level, and locations far from buildings, walls, and other obstacles were chosen to reduce the local influence of air currents. The measurements were made under relatively stable meteorological conditions. The measurements were carried out based on the active aerosol-filter sampling principles of the ASTM D6327-10 standard (ASTM International 2016), and the outdoor measurements were performed in accordance with the recommendations of the RADONORM project (RADONORM Consortium 2024).

Determination of long-lived alpha activity (LLAA) in airborne aerosols

The LLAA present in airborne aerosol particles was determined by filter sampling followed by alpha-radiometric analysis. Samples were drawn through an AFA-RSP filter using an aspiration pump placed 1 m above the ground at a rate of 312.5 L min^{-1} for 16 minutes. The volume of air filtered for each sample was 5 m^{3}. After sampling, the filters were stored under laboratory conditions for 5 days. This period is sufficient for the complete decay of the short-lived decay products of radon and thoron (Jha et al. 2000).

The total alpha activity on the aerosol filters was measured using a "Progress-AR" alpha radiometer (NPP "Doza", Russian Federation). The instrument is equipped with a ø60 × 60 mm ZnS(Ag) scintillation detector and is capable of

recording alpha particles in the 1.5–8 MeV energy range. The minimum detection limit of the instrument is 9×10^{-3} Bq, and the relative measurement error does not exceed ±10% (Nazarov et al. 2023; SPC Doza n.d.).

Before the measurements, the instrument was checked using standard reference sources, and the background values were taken into account. The alpha activity on the filters was processed using the "Progress" software, and the LLAA values were calculated in mBq m^{-3} relative to the volume of filtered air.

Measurement of the ambient dose equivalent rate

The ambient dose equivalent rate of gamma radiation, H*(10), was determined using a DKS-96 dosimeter-radiometer (NPP "Doza", Russian Federation) (Doza 2012). The measurements were made with a UIK-05-01 console and a connected BDPG-96 gamma-detection unit. The unit is based on a ø25 × 40 mm NaI(Tl) scintillation detector, with a sensitivity calibrated against ^{137}Cs of 500 (counts s^{-1})/(μSv h^{-1}). The measurement range is 0.05–100 μSv h^{-1}, the energy threshold is 50 keV, and the main relative error is ±13%. Before each measurement series, the instrument was checked in accordance with the valid annual calibration certificate.

H*(10) was measured at the control points and at the sorption sites, in both open and indoor environments, at a height of 1 m above ground level. In the open environment, up to five repeated measurements were taken within a circle of 3 m radius around each point, and indoors the measurements were made in several rooms. For each object, the range of minimum and maximum values was reported as the final result (Bakhtin et al. 2025; Lesbek et al. 2025; Yılmazkaya et al. 2025). A height of 1 m corresponds approximately to the average level of the most radiosensitive organs in the human body (Ateş et al. 2020).

Surface alpha contamination measurement

The surface alpha contamination density was determined using the BDZA-96 alpha-radiation detection unit of the DKS-96 dosimeter-radiometer. The unit is based on a ZnS(Ag) scintillation detector with an active surface area of 70 cm^2 and, calibrated against the ^{239}Pu nuclide, records the count rate of alpha particles in the range from 0.1 to 1×10^4 min^{-1} cm^{-2}. The measurements were carried out on the surfaces of technological equipment and on the floor and wall surfaces of the corresponding production rooms. For each piece of equipment and each surface, measurements were taken at 3–5 control points. With the detection unit held approximately 0.5–1 cm from the surface, the result was recorded at each point over a fixed time interval of 20 s. Before each measurement, the instrument's automatic background compensation function was activated. The instrument determined the background level over 60 s and automatically subtracted it from the subsequent measurement result. From the values obtained for each piece of equipment and each surface, the minimum and maximum results were selected and reported as a range (min–max).

To convert the count rate (min^{-1} cm^{-2}) into activity density (Bq cm^{-2}), the ISO 7503-1:2016 standard and the general expression for the assessment of surface contamination were used (CNSC 2023; ISO 2016):

$$A = \frac{N - N_b}{60 \cdot \varepsilon \cdot S \cdot F} \qquad (1)$$

where A is the surface activity density (Bq cm^{-2}); N is the total count rate (min^{-1}); N_b is the background count rate (min^{-1}); ε is the radionuclide-specific detection efficiency of the detection unit; S is the active surface area of the detector (cm^2); F is the pick-up factor; and 60 is the coefficient for converting minutes to seconds.

Under the conditions of this study, expression (1) was simplified. Owing to the automatic background compensation, the background term was subtracted by the instrument ($N_b = 0$); because the measurements were made by the direct method, the pick-up factor F = 1; and because the count rate was recorded directly normalized to the detector surface (R_s, min^{-1} cm^{-2}), the surface term (S) was not introduced separately:

$$A = \frac{R_s}{60 \cdot \varepsilon} \qquad (2)$$

where R_s is the background-subtracted count rate normalized to the active surface area of the detector (min^{-1} cm^{-2}); ε is the detection efficiency. Because the study object is associated with natural uranium, the ε value was adopted based on the passport efficiency of the BDZA-96 unit for the ^{238}U isotope – 15% (ε = 0.15) (for ^{234}U the passport efficiency is 25%) (Doza 2012). It should be emphasized that, because the instrument is calibrated against the ^{239}Pu nuclide, the Bq cm^{-2} values calculated using the ^{238}U efficiency are approximate and are intended for comparison with other sources only at the order-of-magnitude level.

Soil sampling and gamma-spectrometric analysis

Soil samples were taken from the surface (0–5 cm) layer of the six USS and eight control points. Each sample of approximately 2 kg was collected using a plastic scoop, placed in polyethylene bags, and labelled. Before laboratory analysis, the samples underwent a preliminary treatment stage. Organic residues and large stone fragments were removed, and the samples were passed through a 5 mm sieve. The samples were then dried, first spread in open air and then in a drying oven at 110 °C for 24 hours until a constant dry weight was reached. The dried samples were placed in standard Marinelli-type plastic containers, hermetically sealed, and stored for 30 days. This period is considered sufficient for secular equilibrium to be established between ^{226}Ra and ^{232}Th and their short-lived decay products (IAEA 1989).

The specific activity of the natural radionuclides (^{226}Ra, ^{232}Th, and ^{40}K) in the soil samples was measured using an MKS-AT1315 gamma-beta spectrometer manufactured by ATOMTEX (ATOMTEX 2020). The instrument is equipped with a ø63 × 63 mm NaI(Tl) scintillation detector and operates in the gamma-radiation energy range from 50 keV to 3 MeV.

The permissible relative error limit of the spectrometer is ±20%, and its energy resolution (662 keV, ^{137}Cs) is 8%. A 1024-channel amplitude analyzer is connected to the instrument. Specialized ATWin software was used for data acquisition and processing. The ^{226}Ra activity was determined from the ^{214}Pb (351 keV) and ^{214}Bi (609 keV, 1120 keV) gamma lines, the ^{232}Th activity from the ^{208}Tl (583 keV, 2614 keV) and ^{212}Pb (239 keV) gamma lines, and the ^{40}K activity directly from the 1460 keV gamma line. Each sample was measured for 2 hours under lead shielding. The recorded spectra were cleaned of background radiation and calibrated using standard samples, and the activity and expanded uncertainty (k = 2) were calculated in the ATWin software.

Assessment of radiation hazard indices

Using the specific activities of the natural radionuclides (^{226}Ra, ^{232}Th, and ^{40}K) determined by the gamma-spectrometric analysis described above, the radiological hazard level of the soils in the study area was assessed. For this purpose, several radiological hazard indicators widely used in international practice were calculated: the radium equivalent activity (Ra_{eq}), the absorbed dose rate (D), and the external (H_{ex}) and internal (H_{in}) hazard indices. These indicators enable quantitative assessment of the potential radiation impact arising from natural radioactivity for the population and production workers (UNSCEAR 2000).

The Ra_{eq} was calculated using the following expression (Akpanowo et al. 2020; Ehsan et al. 2020):

$$Ra_{eq}(Bq\ kg^{-1}) = A_{Ra} + 1.43\,A_{Th} + 0.077\,A_K \quad (3)$$

where A_{Ra}, A_{Th}, and A_K are the specific activities of ^{226}Ra, ^{232}Th, and ^{40}K, respectively.

The absorbed gamma-radiation dose rate in outdoor air ($D_{outdoor}$) at a height of 1 m above ground level was determined as follows (Jananee et al. 2021; Orosun et al. 2021):

$$D_{\text{outdoor}}(nGy\ h^{-1}) = 0.462\,A_{Ra} + 0.604\,A_{Th} + 0.0417\,A_K \quad (4)$$

where the coefficients express the dose-rate contribution per unit activity of the respective radionuclides (nGy h^{-1} / Bq kg^{-1}).

The H_{ex} was calculated to assess the risk of external gamma exposure from the soil (Ehsan et al. 2020):

$$H_{ex} = \frac{A_{Ra}}{370} + \frac{A_{Th}}{259} + \frac{A_K}{4810} \quad (5)$$

where the denominators (370, 259, and 4810 Bq kg^{-1}) represent the permissible limiting activities of the respective radionuclides for external exposure.

The H_{in} accounts for the risk of internal exposure through the inhalation of radon and its decay products (Asaduzzaman et al. 2015):

$$H_{in} = \frac{A_{Ra}}{185} + \frac{A_{Th}}{259} + \frac{A_K}{4810} \quad (6)$$

where the denominator for ^{226}Ra is 185 Bq kg^{-1}. This value accounts for the relatively higher radiotoxicity of radium under internal exposure. H_{ex} and H_{in} are dimensionless quantities.

Statistical analysis

Statistical analysis and figure preparation were performed in Python 3.12 (Google Colab) using the Pandas, NumPy, SciPy, Matplotlib, and Seaborn libraries. Because the data were not normally distributed and the sample size was limited, non-parametric methods were applied.

For EERC and LLAA, differences between the functional zones and the control points were evaluated using the Kruskal–Wallis test. When a significant difference was detected ($p < 0.05$), pairwise comparisons were performed using Dunn's post-hoc test with the Holm correction. Differences between the USS zones and the control points were assessed using the Mann–Whitney U test, and effect sizes were quantified using the rank-biserial correlation coefficient. Because the sample size for H*(10) and surface alpha contamination was limited, only descriptive statistics were applied.

The relationships among indicators were assessed using the Spearman rank correlation coefficient (ρ). This method does not require a normal distribution, is less sensitive to extreme values, and is consistent with the non-parametric approach. For indicators reported as a min–max range (H*(10), surface alpha), the range midpoint was used. In all analyses, a significance criterion of $p < 0.05$ was adopted (Zar 2010).

Results and discussion

Airborne radiological characteristics (EERC and LLAA)

The mean EERC and LLAA values by technological zone are presented in Table 2, and the results for the control points in Table 3.

Table 2 Mean ± SD of EERC and LLAA measured at different technological units of the uranium sorption facility.

Technological unit	**EERC (Bq m^{-3})**	**LLAA (mBq m^{-3})**
Site area	10.8 ± 2.8	9.5 ± 0.9
Resin Exchange Platform (REP)	18.7 ± 2.0	13.18 ± 1.12

Technological unit	EERC (Bq m^{-3})	LLAA (mBq m^{-3})
Sorption Column No. 2 (SC2)	17.0 ± 2.4	13.73 ± 1.48
Sorption Column No. 1 (SC1)	16.3 ± 1.5	13.86 ± 0.90
Water Reservoir (WR)	11.3 ± 2.2	10.43 ± 0.56
Pump Station (PST)	11.3 ± 1.8	10.27 ± 0.88
Operator Room (OPR)	7.7 ± 1.0	6.04 ± 0.48
Canteen (CAN)	6.7 ± 0.8	5.22 ± 0.77

For both indicators, the highest values were recorded at the REP (EERC 18.7 ± 2.0 Bq m^{-3}; LLAA 13.18 ± 1.12 mBq m^{-3}) and in the SC1 and SC2 zones. Values at the Site area, WR, and PST were intermediate, and the lowest results corresponded to the OPR and CAN. The similarity of the EERC and LLAA distributions shows that radon decay products and alpha-active aerosols accumulate mainly in the zones where the technological operations involving uranium solutions and resin are carried out.

Table 3 EERC and LLAA values measured at the residential control points.

Control points	CP-1	CP-2	CP-3	CP-4	CP-5	CP-6	CP-7	CP-8	Mean ± SD
EERC (Bq m^{-3})	4	3	6	4	5	5	4	3	4.3 ± 1.0
LLAA (mBq m^{-3})	4.58	4.44	5.04	4.50	4.47	4.04	4.22	4.75	4.51 ± 0.31

At the control points, EERC was recorded in the range 3–6 Bq m^{-3} (mean 4.3 ± 1.0 Bq m^{-3}) and LLAA in the range 4.04–5.04 mBq m^{-3} (mean 4.51 ± 0.31 mBq m^{-3}). These values are considerably lower than the results in the technological zones, especially at the REP, SC1, and SC2. The differences among the groups were evaluated using the Kruskal–Wallis and Dunn post-hoc tests. The distribution of the EERC values is presented in Fig. 2.

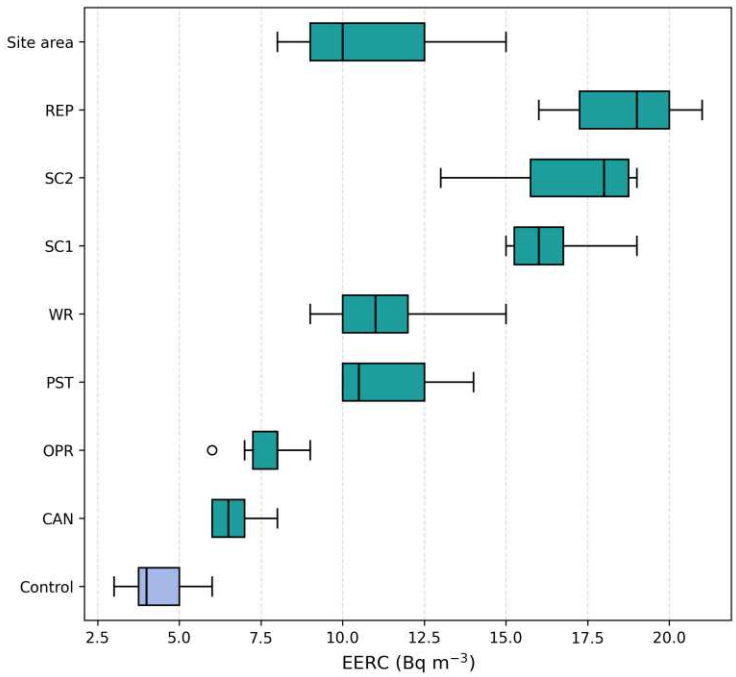

Fig. 2 Distribution of the EERC values measured in the technological zones and at the control points.*

**The boxes represent the interquartile range (IQR), the central line the median, and the "Whiskers" the minimum and maximum values.*

Radon concentration was not uniformly distributed across the functional zones (Fig. 2). The highest median EERC was observed at the REP (≈19 Bq m^{-3}), followed by SC1 and SC2. This is explained by the enhanced emanation of radon from the liquid phase into the air as a result of handling uranium-bearing solutions and sorbents during the technological process. The WR, PST, and Site area showed intermediate levels, while the OPR and CAN showed low values close to those of the control points, reflecting the decrease in EERC with increasing distance from the technological process. Because the geological background in the soil was relatively uniform across all zones (see "Natural radionuclide activity in soils"), the observed differences are associated not with natural activity but with the technological process.

The Kruskal–Wallis test confirmed a significant difference among the groups ($H = 50.03$; $df = 8$; $p < 0.001$). According to the Dunn post-hoc analysis, the values at the REP, SC1, and SC2 were significantly higher than at the control points ($p < 0.05$); the difference at the Site area, although descriptively noticeable, was not statistically confirmed ($p > 0.05$).

The EERC values recorded at the control points were consistent with results obtained in settlements adjacent to uranium-industry areas in Central Asia. In settlements near ISL areas in southern Kazakhstan (Bakhtin et al. 2025), EERC ranged from 33 to 64 Bq m^{-3}, whereas in certain areas of northern Kazakhstan (Kashkinbayev et al. 2025) it reached up to 303–658 Bq m^{-3}. In the present study, too, all EERC values were below the 100 Bq m^{-3} level recommended by the ICRP (ICRP 2014), with the highest values observed in the technological zones of sorption. Because the short-lived decay

products of radon do not fully characterize the radiological state of the air, the LLAA concentration was analyzed at the next stage (Fig. 3).

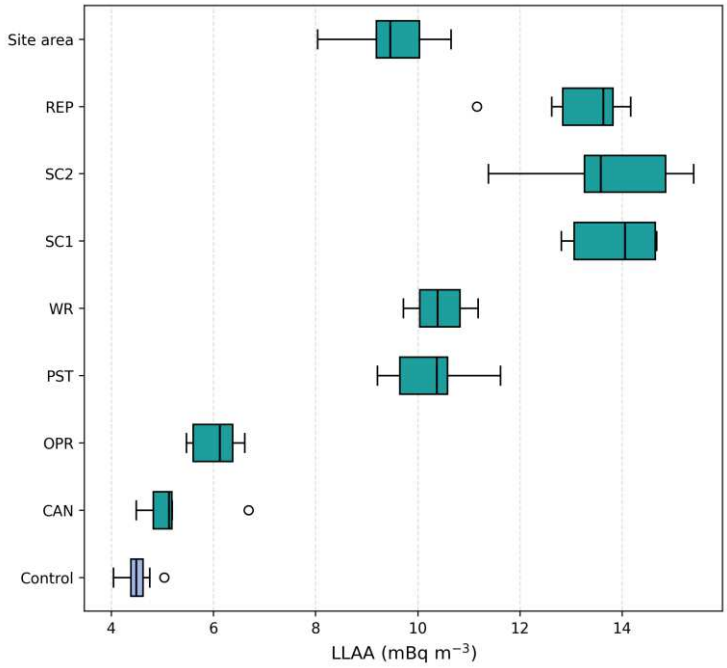

Fig. 3 Distribution of the LLAA measured in the technological units of the uranium sorption facilities and at the control points.

Figure 3 shows the distribution of LLAA across the different technological units. Similar to EERC, the highest median LLAA values were observed at the REP, SC1, and SC2. The relatively wide interquartile ranges indicate greater variability in aerosol concentrations during different stages of the technological process. Elevated LLAA levels result from the attachment of radon progeny to airborne aerosol particles, which promotes their accumulation in the workplace air. This process represents the transition of radionuclides from the gaseous to the particulate (aerosol) phase of the migration chain. In addition, mechanical operations during resin exchange further increase aerosol generation. In contrast, the OPR, CAN, and site area showed consistently low and stable LLAA values because these locations are separated from the technological process and are farther from the main sources of radioactive aerosols.

The Kruskal–Wallis test confirmed significant differences in LLAA among the technological units ($H = 50.66$, $df = 8$, $p < 0.001$). Dunn's post-hoc analysis showed that LLAA values at the REP, SC1, and SC2 were significantly higher than those at the control points ($p < 0.05$), whereas the Site area did not differ significantly from the control points ($p > 0.05$). Furthermore, LLAA at the REP was significantly higher than at the CAN, while SC1 and SC2 showed significantly higher values than both the CAN and the OPR ($p < 0.05$). Because airborne radionuclide concentrations alone do not fully characterize the radiation environment, the external gamma radiation level, expressed as H*(10), was evaluated in the next stage.

Ambient gamma dose equivalent rate, H*(10)

To characterize the external gamma-radiation level of the study area, H*(10) was measured in all zones and at all control points. The results were recorded as a min–max range and analyzed using descriptive statistics (Fig. 4).

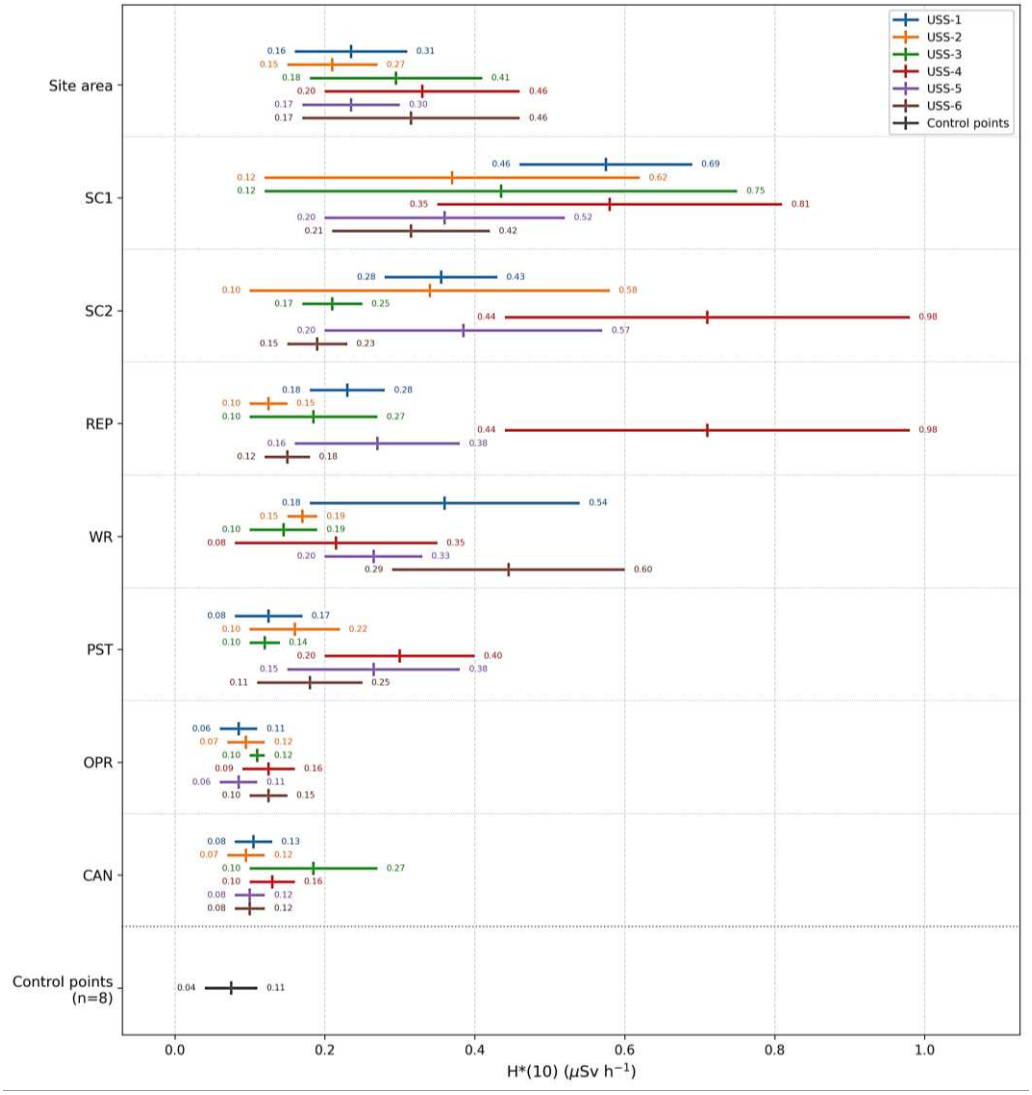

Fig. 4 Ranges of the H*(10) values measured in the technological zones and at the control points.*

**For each point, the horizontal line represents the min–max range and the central mark the midpoint. Colors correspond to each site (USS-1–USS-6).*

The highest and widest ranges were recorded at the sorption columns (SC1: 0.12–0.81; SC2: 0.10–0.98 μSv h^{-1}) and at the resin exchange platform (REP: 0.10–0.98 μSv h^{-1}). The Site area, WR, and PST showed intermediate levels, while the CAN (0.07–0.27 μSv h^{-1}) and OPR (0.06–0.16 μSv h^{-1}) showed values closest to the control-point level (0.04–0.11 μSv h^{-1}). To quantitatively assess differences between the zones and the background, the mean H*(10) value for each unit was calculated relative to the mean value at the control points (Fig. 5).

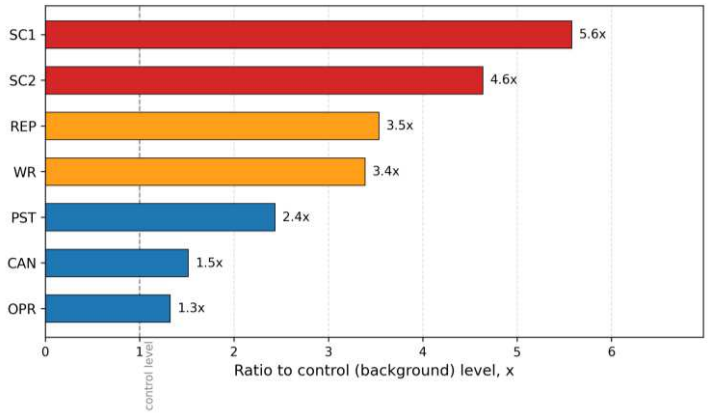

Fig. 5 Ratio of the mean H*(10) value of the technological zones to the background level at the control points.*

**The ratio was calculated by dividing the mean value of each functional zone across all sites by the mean value of the control points. The Site area was excluded from the analysis because it is not considered a technological object.*

The highest ratio was recorded at the sorption columns (5.6 at SC1 and 4.6 at SC2), followed by the REP (3.5), WR (3.4), and PST (2.4). The CAN (1.5) and OPR (1.3) showed values closest to the control points. The spatial distribution of H*(10) was consistent with the EERC and LLAA results: the highest values were again observed at the sorption columns and the resin exchange platform. This consistency shows that the radiological indicators form in the same functional zones and that they are associated with the technological process. The high H*(10) values can be explained by the accumulation of radionuclides on equipment surfaces and by the influence of the technological process.

These results are consistent with studies carried out in other uranium production areas. In areas adjacent to uranium production facilities in southern Kazakhstan, H*(10) was recorded in the range 0.5–1.2 μSv h^{-1} in the technological zones and 0.03–0.15 μSv h^{-1} in the settlements (Bakhtin et al. 2025). In the Taboshar uranium area of Tajikistan, values of 0.3–3.9 μSv h^{-1} were likewise observed in the production areas, whereas in residential buildings they were mostly below 0.2 μSv h^{-1} (Lespukh et al. 2013). In the present study, H*(10) at the control points was 0.04 to 0.11 μSv h^{-1}, with the highest values recorded in the technological zones. This confirms that the spatial distribution of external gamma radiation is closely associated with the intensity of the uranium production process.

Surface alpha contamination

Surface alpha contamination reflects a stage of radionuclide dispersion distinct from the airborne and external radiation pathways, namely the deposition of alpha-emitting radionuclides onto the surfaces of technological equipment and production rooms. Whereas EERC, LLAA, and H*(10) characterize radionuclides in the air and the external radiation field, surface alpha contamination reflects the local accumulation of radionuclides on solid surfaces in direct contact with uranium-bearing process solutions, thereby complementing the source-attribution analysis.

Surface alpha contamination is measured in the uranium industry mainly within the framework of internal radiation control (IAEA 2020) and is rarely analyzed in independent scientific publications. Presenting it within a single framework together with the other three indicators enables to assess the distribution of radionuclides across the airborne, external-radiation, and surface phases in an integrated manner. The minimum and maximum measured values are presented in Fig. 6.

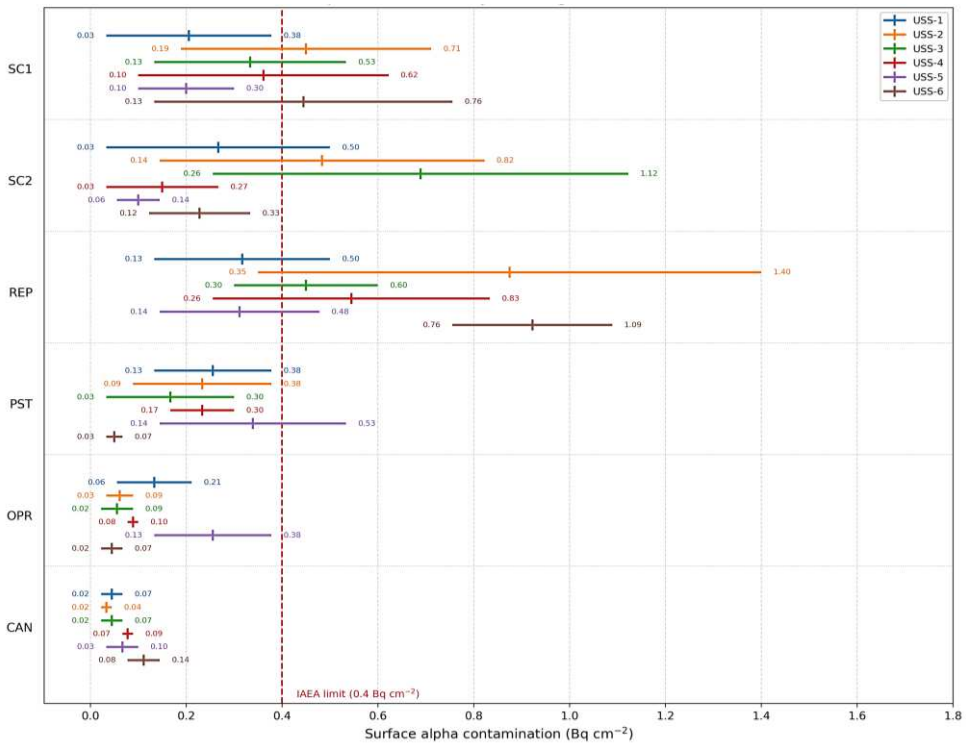

Fig. 6 Ranges of the surface alpha contamination values measured across the technological zones.*

**For each point, the horizontal line represents the min–max range and the central mark the midpoint. The colour corresponds to each site (USS-1–USS-6). The dashed red line indicates the contamination criterion (0.4 Bq cm^{-2}) set by the IAEA for low-toxicity alpha emitters, including natural uranium* (IAEA 2018).

As can be seen from Fig. 6, the level of surface alpha contamination differed considerably depending on the type of technological equipment. The highest and widest ranges were recorded at the resin exchange platform (REP: 0.13–1.40 Bq cm^{-2}) and at sorption column No. 2 (SC2: 0.03–1.12 Bq cm^{-2}); at SC1 the values were in the range 0.03–0.76 Bq cm^{-2}. At the pump station, the indicators remained intermediate (PST: 0.03–0.53 Bq cm^{-2}), and the lowest and narrowest ranges were observed at the operator room (OPR: 0.02–0.38 Bq cm^{-2}) and the canteen (CAN: 0.02–0.14 Bq cm^{-2}). This distribution corresponds to the trend identified in the EERC, LLAA, and H*(10) results.

Comparison of the obtained results with the surface contamination criterion recommended by the IAEA (0.4 Bq cm^{-2}) showed that at many measurement points in the REP, SC1, and SC2 zones the values exceeded this criterion, and these surfaces were classified as contaminated. The highest value recorded at the REP (1.40 Bq cm^{-2}) was 3.5 times higher than

the criterion. At the PST, an exceedance was observed at only one site (USS-5). All values at the OPR and CAN were below the criterion, and these surfaces were assessed as uncontaminated.

Measured surface alpha values at operating uranium enterprises are almost absent from the open literature; the available quantitative data mainly concern facilities at the decommissioning stage. At the UDG gaseous-diffusion enrichment plant in Pierrelatte, France (operational in 1960–1996, now under decommissioning), the uranium surface activity measured by gamma spectrometry was 7.47 ± 0.75 and 16.6 ± 6.0 Bq cm^{-2} at various points, mainly attributable to ^{234}U and ^{238}U (Salvador et al. 2023, 2024). Owing to differences in measurement methods, these values cannot be compared directly; however, an order-of-magnitude comparison indicates that the contamination level at the operating USS (maximum 1.40 Bq cm^{-2}) is considerably lower than at a legacy facility that has not been fully decontaminated.

Surface alpha contamination reflects the final stage of radionuclide dispersion, namely the deposition of radionuclides onto surfaces. Whereas EERC and H*(10) characterize radon release into the air and the associated external gamma radiation, surface alpha contamination reflects the accumulation of radionuclides on the surfaces of equipment that come into direct contact with uranium-bearing solutions and ion-exchange resins.

The simultaneous occurrence of high EERC, LLAA, H*(10), and surface alpha contamination values in the REP, SC1, and SC2 zones indicates the predominance of the technological-process influence and the more intensive accumulation of radionuclides in these zones. This confirms that the observed high values are associated not with the natural geological background but with the technological process of uranium sorption.

Natural radionuclide activity in soils

Along with the atmospheric and surface indicators, the activity concentrations of natural radionuclides in the soil were also assessed. Soil ^{226}Ra governs radon exhalation, whereas ^{232}Th and ^{40}K, together with ^{226}Ra, control the external gamma dose rate. Collectively, these radionuclides define the natural radiological background.

If the activity of soil radionuclides in the USS zones does not differ considerably from that at the control points, it indicates that the elevated indicators identified in the previous sections reflect the predominant influence of the technological process rather than the geological background. The results are presented in Table 4.

Table 4 Activity of the natural radionuclides ^{40}K, ^{226}Ra, and ^{232}Th in soil at the USS and control points.

Sampling location	^{40}K (Bq kg^{-1})	^{226}Ra (Bq kg^{-1})	^{232}Th (Bq kg^{-1})
USS-1	555 ± 61	36 ± 3	39 ± 4
USS-2	541 ± 55	35 ± 4	35 ± 4
USS-3	531 ± 51	71 ± 6	37 ± 3

Sampling location	^{40}K (Bq kg^{-1})	^{226}Ra (Bq kg^{-1})	^{232}Th (Bq kg^{-1})
USS-4	562 ± 60	46 ± 5	38 ± 5
USS-5	892 ± 91	40 ± 5	21 ± 3
USS-6	683 ± 69	40 ± 4	39 ± 5
CP-1	592 ± 62	29 ± 3	31 ± 4
CP-2	627 ± 66	35 ± 3	31 ± 4
CP-3	486 ± 51	52 ± 5	26 ± 3
CP-4	539 ± 58	31 ± 3	30 ± 4
CP-5	581 ± 62	43 ± 4	36 ± 5
CP-6	467 ± 49	28 ± 2	36 ± 4
CP-7	474 ± 50	38 ± 4	26 ± 3
CP-8	547 ± 56	37 ± 4	26 ± 4

No large difference in the activity of ^{40}K, ^{226}Ra, and ^{232}Th in the soils was observed between the USS-1–USS-6 technological zones and the CP-1–CP-8 control points. The ^{40}K values were in the range 531–892 Bq kg^{-1} (mean 627.3 Bq kg^{-1}) in the USS zones and 467–627 Bq kg^{-1} (mean 539.1 Bq kg^{-1}) at the control points. For ^{226}Ra, the values were 35–71 Bq kg^{-1} (mean 44.7 Bq kg^{-1}) and 28–52 Bq kg^{-1} (mean 36.6 Bq kg^{-1}), respectively, and for ^{232}Th, 21–39 Bq kg^{-1} (mean 34.8 Bq kg^{-1}) and 26–36 Bq kg^{-1} (mean 30.2 Bq kg^{-1}). Although the mean values in the USS zones were approximately 15–22% higher than at the control points for all three nuclides, this difference is much smaller than the several-fold differences observed in the atmospheric and surface indicators.

The comparison among the USS zones also did not confirm a technological-impact pattern. The highest ^{40}K value (892 Bq kg^{-1}) was recorded at USS-5 and the highest ^{226}Ra value (71 Bq kg^{-1}) at USS-3, both zones that were intermediate or low in the airborne indicators. Thus, the differences in the soil can be explained by the individual geological characteristics of each point rather than by the level of technological activity.

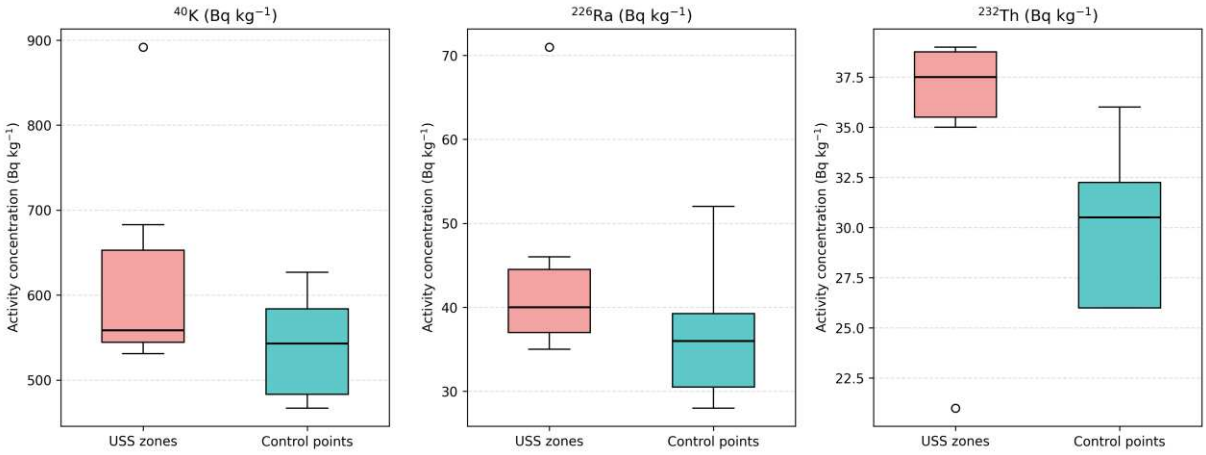

Fig. 7 Distribution of ^{40}K, ^{226}Ra, and ^{232}Th activity in the soils of the USS zones and control points.

The box plots presented in Fig. 7 visually reflect the observations in Table 4. Although the medians of the USS zones for ^{40}K and ^{226}Ra (558.5 and 40.0 Bq kg^{-1}, respectively) are slightly higher than the medians of the control points (543.0 and 36.0 Bq kg^{-1}), the interquartile ranges of the two groups partly overlap, indicating the small size of the difference between the groups. For ^{232}Th, the median of the USS group (37.5 Bq kg^{-1}) is higher than that of the control group (30.5 Bq kg^{-1}), so the difference between the groups is more clearly manifested for this indicator. Nevertheless, the low value at USS-5 (21 Bq kg^{-1}) stands out as a separate point in the plot and can be explained by a local geological feature. The single high deviations in the ^{40}K and ^{226}Ra plots (892 Bq kg^{-1} at USS-5 and 71 Bq kg^{-1} at USS-3) show that these two zones have particular geological characteristics. However, these deviations are not associated with technological activity. The fact that these zones were at intermediate or low levels in the airborne indicators shows that no systematic technological impact was observed.

Environmental radiological risk

To assess the combined radiological impact of natural radionuclides in the soil, the Ra_{eq}, $D_{outdoor}$, H_{ex}, and H_{in} values were calculated. Ra_{eq} and $D_{outdoor}$ express the overall gamma-radiation potential of a site in physical units (Bq kg^{-1} and nGy h^{-1}, respectively), while H_{ex} and H_{in} characterize the radiation hazard relative to internationally recommended limit values (= 1). H_{in} also accounts for the additional hazard arising from the inhalation of radon. The results are presented in Figs. 8 and 9.

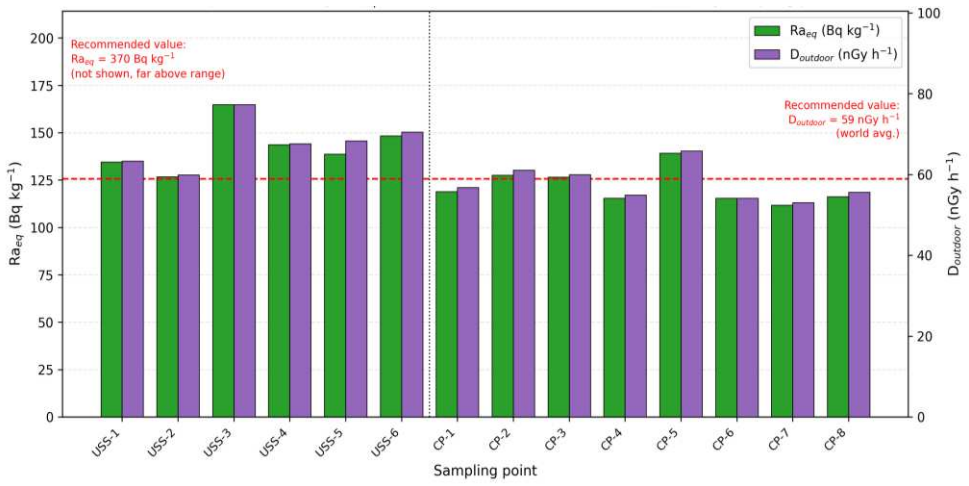

Fig. 8 Distribution of the Ra_{eq} and $D_{outdoor}$ values in the soil across the sampling points.*

**The dashed red line indicates the recommended world average value for $D_{outdoor}$ (59 nGy h^{-1}); the recommended value for Ra_{eq} (370 Bq kg^{-1}) is not shown separately in the plot because it is much higher than all observed values.*

As can be seen from Fig. 8, the Ra_{eq} values at all 14 points were considerably below the internationally recommended limit (370 Bq kg^{-1}): 126.7–164.8 Bq kg^{-1} (mean 142.8 ± 13.1) in the USS zones and 111.7–139.2 Bq kg^{-1} (121.4 ± 9.1) at the control points. For $D_{outdoor}$, the situation is different: the values were 59.9–77.3 nGy h^{-1} (67.8 ± 6.0) and 53.0–65.8 nGy h^{-1} (57.7 ± 4.3), respectively, exceeding the world average value reported by UNSCEAR (59 nGy h^{-1}) in all six USS zones and at three control points (CP-2, CP-3, CP-5). The value 59 nGy h^{-1} is a worldwide average background value and is not a safety limit. Because Ra_{eq} and $D_{outdoor}$ are calculated from the same combination of radionuclides, they showed a similar spatial distribution at all points (a USS/control ratio of 1.18 for both). The highest values were recorded at USS-3 (Ra_{eq} = 164.8 Bq kg^{-1}; $D_{outdoor}$ = 77.3 nGy h^{-1}), which is associated with the high ^{226}Ra activity in this zone (71 Bq kg^{-1}); even so, Ra_{eq} remained more than two times below the limit.

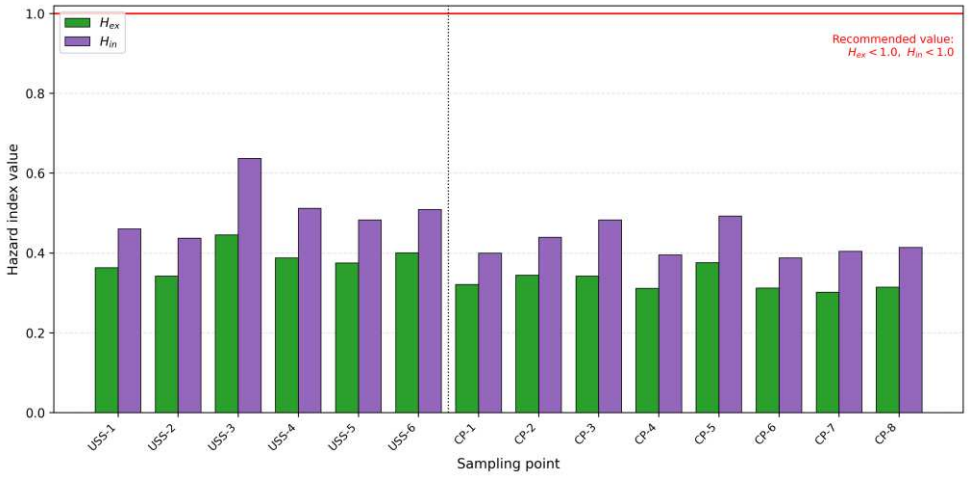

Fig. 9 Distribution of the external (H_{ex}) and internal (H_{in}) radiation hazard indices across the sampling points. The red line indicates the internationally recommended limit value (= 1) for H_{ex} and H_{in}.

According to Fig. 9, the H_{ex} and H_{in} values at all 14 points were several times below the limit (= 1), reflecting a radiologically satisfactory situation. In the USS zones, H_{ex} was in the range 0.342–0.445 (mean 0.386 ± 0.035) and H_{in} in the range 0.437–0.637 (0.506 ± 0.070); at the control points, values of 0.302–0.376 (0.328 ± 0.025) and 0.387–0.492 (0.427 ± 0.040), respectively, were recorded. The fact that H_{in} is higher than H_{ex} at all points is explained by the greater weight given in the formula to the inhalation exposure to radon. The highest H_{in} value (0.637) again corresponds to USS-3, showing its association with the high ^{226}Ra activity. However, this value is considerably below the limit.

According to the Mann–Whitney U test, the Ra_{eq}, $D_{outdoor}$, H_{ex}, and H_{in} values differed significantly between the USS and control groups ($p = 0.008–0.020$). However, the practical magnitude of this difference is small: the USS means are only ≈18% higher than the control level, and the effect size (rank-biserial $r = 0.75–0.83$) is several times smaller than the difference observed in the EERC, LLAA, and H*(10) indicators (150%, 111%, and 231%, respectively; $r = 1.0$ – the groups completely separated). Thus, all soil indicators are far below the international safety limits, and the difference between the USS and control groups is statistically significant but practically small. These results support the hypothesis that the observed elevated radiation indicators are associated mainly with the technological process.

Correlation analysis among the radiological indicators

In the previous sections, it was found that the radiation indicators were consistently increased in the technological zones, whereas the soil radionuclides showed a relatively small difference. To quantitatively assess these relationships, Spearman correlation analysis was carried out in three stages. In the first stage, the radiation indicators were compared with one another. Because surface alpha was measured only on the surfaces of technological equipment, the correlations involving it were evaluated at $n = 36$, and those for EERC, LLAA, and H*(10) at $n = 56$. In the second stage, the relationships between soil radionuclides and radiation hazard indices were analyzed ($n = 14$). In the third stage, the cross-group relationships between the radiation indicators and the soil parameters were assessed, quantitatively testing the main hypothesis.

Table 5a EERC, LLAA, H*(10) – Spearman correlation (n = 56).

	EERC	**LLAA**	**H*(10)**
EERC	1		
LLAA	0.916***	1	
H*(10)	0.764***	0.825***	1

Table 5b Correlation matrix including surface alpha – Spearman correlation (n = 36).

	EERC	LLAA	H*(10)	Surface alpha
EERC	1			
LLAA	0.807***	1		
H*(10)	0.695***	0.798***	1	
Surface alpha	0.760***	0.699***	0.477**	1

** p < 0.05; ** p < 0.01; *** p < 0.001.*

According to Table 5a, strong and statistically significant positive correlations were found for all pairs among EERC, LLAA, and H*(10) (ρ = 0.764–0.916; p < 0.001). The strongest relationship was recorded between EERC and LLAA (ρ = 0.916), showing that radon and its long-lived decay products have a common source. The relatively lower but still strong correlation of H*(10) with EERC and LLAA (ρ = 0.764 and 0.825) shows that the external gamma radiation exhibits a similar spatial distribution, but that its source also includes surfaces and structures beyond the air.

The results with surface alpha contamination added (n = 36), presented in Table 5b, confirm the same pattern: surface alpha showed a strong correlation with EERC (ρ = 0.760; p < 0.001), a moderate-to-strong correlation with LLAA (ρ = 0.699; p < 0.001), and a weaker but significant relationship with H*(10) (ρ = 0.477; p < 0.01). The lower coefficient with H*(10) is an expected result: these two quantities characterize different stages of migration (external radiation and deposition on the surface). Overall, the consistent correlations among the four indicators show a common dispersion pattern of radionuclides associated with the technological process.

Table 6 Spearman correlation between soil parameters and radiation hazard indices (n = 14).

	^{40}K	^{226}Ra	^{232}Th	Ra_{eq}	$D_{outdoor}$	H_{ex}	H_{in}
^{40}K	1						
^{226}Ra	0.062	1					
^{232}Th	0.111	0.091	1				
Ra_{eq}	0.534*	0.645*	0.594*	1			
$D_{outdoor}$	0.578*	0.674**	0.465	0.978***	1		
H_{ex}	0.534*	0.645*	0.594*	1.000***	0.978***	1	
H_{in}	0.393	0.872***	0.414	0.930***	0.930***	0.930***	1

** p < 0.05; ** p < 0.01; *** p < 0.001.*

According to Table 6, ^{40}K, ^{226}Ra, and ^{232}Th in the soil showed weak and statistically non-significant correlations with one another ($\rho = 0.062–0.111$; $p > 0.05$; $n = 14$). This result supports the earlier observation that the distribution of soil radionuclides is determined by independent geological factors.

As expected, the radiation hazard indices showed very strong correlations with one another ($\rho = 0.930–1.000$; $p < 0.001$), including a perfect relationship between Ra_{eq} and H_{ex} ($\rho = 1.000$; because H_{ex} is a direct linear expression of Ra_{eq}). This result is explained by the fact that Ra_{eq}, H_{ex}, $D_{outdoor}$, and H_{in} are calculated from the same radionuclides and does not imply an independent physical relationship. All indices showed the strongest correlation with ^{226}Ra ($\rho = 0.645–0.872$), while the relationships with ^{40}K and ^{232}Th were weaker ($\rho = 0.393–0.594$). This difference is explained by the higher weight of the ^{226}Ra contribution in the index formulas.

Table 7 Cross-group Spearman correlation between the external radiological indicators and the soil parameters (n = 14, at the Site-area level).

	^{40}K	**^{226}Ra**	**^{232}Th**	**Ra_{eq}**	**$D_{outdoor}$**	**H_{ex}**	**H_{in}**
EERC	0.228	0.532	0.522	0.722**	0.722**	0.722**	0.707**
LLAA	0.490	0.502	0.315	0.701**	0.758**	0.701**	0.692**
H*(10)	0.313	0.337	0.643*	0.734**	0.680**	0.734**	0.628*

** $p < 0.05$; ** $p < 0.01$.*

According to Table 7, statistically significant, moderate-to-strong correlations were found between EERC, LLAA, and H*(10) and the radiation hazard indices ($\rho = 0.628–0.758$; $p < 0.05$). The relationships with the raw radionuclides were weaker ($\rho = 0.228–0.643$), and a significant correlation was recorded only between H*(10) and ^{232}Th ($\rho = 0.643$; $p = 0.013$).

However, these results should be interpreted with caution. When the USS ($n = 6$) and control ($n = 8$) groups were analyzed separately, all correlations lost their statistical significance ($p > 0.05$). This shows that the high correlations observed for $n = 14$ mainly reflect the overall level difference between the USS and control groups. In addition, because the soil samples were taken only from the Site area, the analysis does not cover the maximum values in the SC1, SC2, and REP zones.

Thus, the correlation analysis shows the consistent interrelationship among the radiation indicators and their association with a common technological source. In contrast, the soil radionuclides showed a relatively independent geological distribution, and the cross-group correlations are explained mainly by the overall level difference between the USS and control groups.

Conclusion

This study provided the first integrated assessment of air, external radiation, surface, and soil indicators across the functional zones of operating USS in Uzbekistan and showed that the elevated radiological levels observed are attributable to the technological process.

For the four independent indicators, EERC, LLAA, H*(10), and surface alpha contamination, the highest values accumulated in the same zones, namely the resin exchange platform and the sorption columns; in these zones, the surface alpha contamination exceeded the IAEA criterion. The strong correlations among the indicators and their consistently elevated levels in the same zones show that these operations are the principal source of the radiological impact.

In contrast, the activity of natural radionuclides in the soil and all hazard indices calculated from them remained well below the internationally recommended limits, while the difference between the USS and control groups was practically small. The correlations observed when both groups were analyzed together were not present within either group separately, indicating that they were primarily driven by the overall differences in variable levels between the USS and the control points. Thus, the technogenic impact is currently localized in the air and surface compartments, and no appreciable migration to the soil was observed.

In practical terms, these results call for occupational radiation protection to be directed to the zones where the highest exposures were recorded: the workers operating at the resin exchange platform and at the sorption columns. Future studies are recommended to assess seasonal variability, vertical migration through the soil profile, and the individual dose burden of workers.

Acknowledgements The authors thank the staff of the Central Research Laboratory of the Navoi Mining and Metallurgical Combinat Joint-Stock Company for technical support and access to laboratory equipment.

Author Contributions Material preparation and data collection were performed by Umidjon Haydarov, Amrullo Muzafarov, Alisher Jurakulov and Dilfuza Sidiqova. Data analysis and review were performed by Umidjon Haydarov, Amrullo Muzafarov, and Diyor Khazratov. The manuscript was written by Umidjon Haydarov and Amrullo Muzafarov. The study was supervised by Amrullo Muzafarov. All authors read and approved the final manuscript.

Funding No funding was received to conduct this study.

Data Availability The data supporting the findings of this study are available from the corresponding author upon reasonable request. Because the facility is a strategic uranium production enterprise and is subject to the enterprise's information-security requirements, the exact coordinates and the names of the settlements are not publicly disclosed. Nevertheless, all relevant data used in the analysis and interpretation are presented within the article.

Statements and Declarations

Ethical Approval Not applicable.

Consent to Participate Not applicable.

Consent to Publish Not applicable.

Competing Interests The authors declare no competing interests.

References

Akpanowo, M., Umaru, I., Iyakwari, S., Joshua, E. O., Yusuf, S., & Ekong, G. B. (2020). Determination of natural radioactivity levels and radiological hazards in environmental samples from artisanal mining sites of Anka, North-West Nigeria. *Scientific African*, *10*, e00561. https://doi.org/10.1016/j.sciaf.2020.e00561

Allaberganova, G., Pulatov, X., Urunov, I., & Muzafarov, A. (2023). Factors increase in background radiation at uranium production facilities. *E3S Web of Conferences*, *417*, 01007. https://doi.org/10.1051/e3sconf/202341701007

Asaduzzaman, K., Mannan, F., Khandaker, M. U., Farook, M. S., Elkezza, A., Amin, Y. B. M., et al. (2015). Assessment of Natural Radioactivity Levels and Potential Radiological Risks of Common Building Materials Used in Bangladeshi Dwellings. *PLOS ONE*, *10*(10), e0140667. https://doi.org/10.1371/journal.pone.0140667

ASTM International. (2016). *Standard Test Method for Determination of Radon Decay Product Concentration and Working Level in Indoor Atmospheres by Active Sampling on a Filter* (No. D6327-10). West Conshohocken, PA: ASTM International.

Ateş, N. Z., Bayrak, K., Turgay, M. E., & Kam, E. (2020). Evaluation of excess lifetime cancer risk caused by external exposure due to natural radioactivity in Bolu, Turkey. *Sigma Journal of Engineering and Natural Sciences*, *38*(2), 945–954.

ATOMTEX. (2020). *MKS-AT1315 Gamma-Beta Spectrometer: Technical Specifications*. Minsk, Belarus: ATOMTEX. https://atomtex-usa.com/product/at1315-gamma-beta-spectrometer/. Accessed 26 May 2026

Bakhtin, M., Ibrayeva, D., Kashkinbayev, Y., Aumalikova, M., Altaeva, N., Tazhedinova, A., et al. (2025). Environmental Monitoring in Uranium Deposit and Indoor Radon Survey in Settlements Located near Uranium Mining Area, South Kazakhstan. *Atmosphere*, *16*(5), 536. https://doi.org/10.3390/atmos16050536

CNSC. (2023). Radioisotope Safety — Monitoring for Radioactive Contamination. Canadian Nuclear Safety Commission. https://www.cnsc-ccsn.gc.ca/eng/nuclear-substances/licensing-class-ii-nuclear-facilities-and-prescribed-equipment/information-class-ii-licensed-facilities/radioisotope-safety-monitoring-contamination/. Accessed 1 July 2026

Doza. (2012). *Dosimeter/Radiometer DKS-96: User Manual*. Moscow, Russia: Scientific Production Company "Doza" (NPP "Doza"). https://www.doza.ru/docs/eng/DKS_96.pdf. Accessed 15 July 2026

Egemberdieva, A. D., Kamchybekova, K. D., Mamaturaimova, N. A., Pirmatova, Z. T., & Dyikanov, K. A. (2025). Radiation Pollution and Public Health Impacts in Mailuu-Suu, Kyrgyzstan. *Journal of Environmental & Earth Sciences*, *7*(8), 363–375. https://doi.org/10.30564/jees.v7i8.10588

Ehsan, M. S., Rahman, M. F., Tabassum, N., Prodhan, M. M. H., Pervin, S., Siraz, M. M., et al. (2020). The Activity Concentration of Radionuclides (226Ra, 232Th and 40K) in Soil Samples and Associated Health Hazards in Natore, Kushtia and Pabna District of Bangladesh. *Journal of Bangladesh Academy of Sciences*, *43*(2), 169–180. https://doi.org/10.3329/jbas.v43i2.45738

Gulomov, P., & Vahobov, H. (2017). *Natural Geography of Uzbekistan*. Tashkent: O'qituvchi.

Haydarov, U., Muzafarov, A., & Khasanov, S. (2026). Radionuclide migration and correlation in the soil–water–air environment at a radioactive waste storage site, Uzbekistan. *Journal of Radioanalytical and Nuclear Chemistry*. https://doi.org/10.1007/s10967-026-10977-y

IAEA. (1989). *Measurement of Radionuclides in Food and the Environment: A Guidebook*. Vienna, Austria: International Atomic Energy Agency.

IAEA. (1997). *Changes and Events in Uranium Deposit Development, Exploration, Resources, Production and the World Supply-Demand Relationship* (No. 961). Vienna: International Atomic Energy Agency.

IAEA. (2005). *Guidebook on Environmental Impact Assessment for In Situ Leach Mining Projects* (IAEA-TECDOC No. 1428). Vienna: International Atomic Energy Agency. https://www.iaea.org/publications/7095/guidebook-on-environmental-impact-assessment-for-in-situ-leach-mining-projects

IAEA. (2018). *Regulations for the Safe Transport of Radioactive Material* (IAEA Safety Standards Series No. SSR-6 (Rev. 1)). Vienna: International Atomic Energy Agency. https://www.iaea.org/publications/11087/regulations-for-the-safe-transport-of-radioactive-material

IAEA. (2020). *Occupational Radiation Protection in the Uranium Mining and Processing Industry* (No. 100). Vienna: International Atomic Energy Agency. https://www.iaea.org/publications/14764/occupational-radiation-protection-in-the-uranium-mining-and-processing-industry

Ibragimov, L. (2016). Importance of studying natural and geographical potential of regions in economic-geographical research (A case study of Samarkand Region). *Nauka i Mir*, *2*(7), 111–115.

ICRP. (2014). Radiological Protection against Radon Exposure. *Annals of the ICRP*, *43*(3).

ISO. (2016). *ISO 7503-1:2016. Measurement of Radioactivity — Measurement and Evaluation of Surface Contamination — Part 1: General Principles* (No. ISO 7503-1:2016). Geneva, Switzerland: International Organization for Standardization. https://www.iso.org/standard/60522.html

Jananee, B., Rajalakshmi, A., Thangam, V., Bharath, K. M., & Sathish, V. (2021). Natural radioactivity in soils of Elephant hills, Tamilnadu, India. *Journal of Radioanalytical and Nuclear Chemistry*, *329*(3), 1261–1268. https://doi.org/10.1007/s10967-021-07886-7

Jha, S., Ghosh, D. K., & Mishra, U. C. (2000). Assessment of exposure of miners to the α-rays of long-lived radionuclides associated with respirable ore dust in the Jaduguda U mine. *Journal of Environmental Radioactivity*, *48*(3), 317–326. https://doi.org/10.1016/S0265-931X(99)00078-8

Kashkinbayev, Y., Ibrayeva, D., Aumalikova, M., Saifulina, E., Bizhanova, D., Mussayeva, E., et al. (2025). Radon Concentration Survey in Settlements Located in Uranium Mining Territory in Northern Kazakhstan. *International Journal of Environmental Research and Public Health*, *22*(5), 723. https://doi.org/10.3390/ijerph22050723

Khasanov, S., Tukhtaev, U., Mamatkulov, O., Safarov, A., & Afsharipour, S. (2024). Natural radionuclide profiles and radiological risks in soils and rocks of the Koytash–Ugam Range, Uzbekistan. *Environmental Monitoring and Assessment*, *196*(9), 847. https://doi.org/10.1007/s10661-024-13015-0

Kholov, D. M. ugli, Muzafarov, A. M., Kholboev, I., & Hoshimov, K. H. ugli. (2021). Methods of Determination of Radiation Factors and Radioecological Conditions in Navoi Industrial Region. *Turkish Journal of Computer and Mathematics Education (TURCOMAT)*, *12*(7), 1112–1119.

Kreuzer, M., & McLaughlin, J. (2010). Radon. In *WHO Guidelines for Indoor Air Quality: Selected Pollutants*. Geneva: World Health Organization.

Lesbek, A., Omori, Y., Bakhtin, M., Ibrayeva, D., Tokonami, S., Kazhiyakhmetova, B., et al. (2025). Seasonal Variations in Effective Radiation Dose in Residential Buildings of the Akmola Region: Assessing the Impact of Basement Presence and Proximity to Uranium Tailings. *Environments*, *12*(10), 357. https://doi.org/10.3390/environments12100357

Lespukh, E., Stegnar, P., Yunusov, M., Tilloboev, H., Zyazev, G., Kayukov, P., et al. (2013). Assessment of the radiological impact of gamma and radon dose rates at former U mining sites in Tajikistan. *Journal of Environmental Radioactivity*, *126*, 147–155. https://doi.org/10.1016/j.jenvrad.2013.07.019

Li, G., & Yao, J. (2024). A Review of In Situ Leaching (ISL) for Uranium Mining. *Mining*, *4*(1), 120–148. https://doi.org/10.3390/mining4010009

Liu, Y., Zhou, W., Gao, B., Zheng, Z., Chen, G., Wei, Q., & He, Y. (2021). Determination of radionuclide concentration and radiological hazard in soil and water near the uranium tailings reservoir in China. *Environmental Pollutants and Bioavailability*, *33*(1), 174–183. https://doi.org/10.1080/26395940.2021.1951123

Mussayeva, E., Bakhtin, M., & Kurbanova, A. (2026). Environmental Impacts of In Situ Leaching Uranium Mining: A Review. *Environments*, *13*(7), 366. https://doi.org/10.3390/environments13070366

Muzafarov, A. M., Oslopovskiy, S. A., & Sattarov, G. S. (2016). Radiometric investigations of technogenic objects. *Tsvetnye Metally*, 15–19. https://doi.org/10.17580/tsm.2016.02.02

Navoiyuran. (2026a). Company History. Navoiyuran State Enterprise. https://navoiyuran.uz/en/about-us/. Accessed 31 May 2026

Navoiyuran. (2026b). Main Business Activities. Navoiyuran State Enterprise. https://navoiyuran.uz/en/main-activity/. Accessed 1 July 2026

Nazarov, Z., Allaberganova, G., Pulatov, K., & Muzafarov, A. (2023). Radiometric measurements at uranium mined-out sites before their reclamation. *XXI century. Technosphere Safety*, *8*(4), 407–414. https://doi.org/10.21285/2500-1582-2023-4-407-414

NTM-Zashchita Ltd. (2012). *Alpharad Plus-AR: Measuring Complex for Monitoring Radon, Thoron and Their Daughter Products*. Moscow, Russia: NTM-Zashchita Ltd. https://all-pribors.ru/opisanie/49013-12-alfarad-plyus. Accessed 1 July 2026

OECD NEA & IAEA. (2025). *Uranium 2024: Resources, Production and Demand*. Paris and Vienna: OECD Publishing and International Atomic Energy Agency. https://www.oecd-nea.org/jcms/pl_103179/uranium-2024-resources-production-and-demand

Orosun, M. M., Ajibola, T. B., Akinyose, F. C., Osanyinlusi, O., Afolayan, O. D., & Mahmud, M. O. (2021). Assessment of ambient gamma radiation dose and annual effective dose associated with radon in drinking water from gold and lead mining area of Moro, North-Central Nigeria. *Journal of Radioanalytical and Nuclear Chemistry*, *328*(1), 129–136. https://doi.org/10.1007/s10967-021-07644-9

Pandit, P., Mangala, P., Saini, A., Bangotra, P., Kumar, V., Mehra, R., & Ghosh, D. (2020). Radiological and pollution risk assessments of terrestrial radionuclides and heavy metals in a mineralized zone of the siwalik region (India). *Chemosphere*, *254*, 126857. https://doi.org/10.1016/j.chemosphere.2020.126857

Puchkov, A. V., Berezina, E. V., Yakovlev, E. Yu., Hasson, N. R., Druzhinin, S. V., Tyshov, A. S., et al. (2022). Radon Flux Density In Conditions Of Permafrost Thawing: Simulation Experiment. *GEOGRAPHY, ENVIRONMENT, SUSTAINABILITY*, *15*(3), 5–18. https://doi.org/10.24057/2071-9388-2022-023

RADONORM Consortium. (2024). *Measurement Protocol of Radon Progeny Attached and Unattached Fraction: Focus on Graded Approach to Measurement on Underground and Specific Types of Workplaces* (Project Deliverable No. D5.9). European Union Horizon 2020 Programme. https://www.radonorm.eu/wp-content/uploads/file_exchange/D5.9_Measurement-protocol-of-radon-progeny-attached-and-unattached-fraction.pdf

Safarov, A., Safarov, A., Khasanov, S., Umirzakov, E., Proshad, R., Suvanova, S., & Muminov, M. (2023). Evaluation of radon hazards at the rural settlements of Uzbekistan. *Environmental Monitoring and Assessment*, *195*(8), 915. https://doi.org/10.1007/s10661-023-11493-2

Salvador, F., Marchais, T., Pérot, B., Allinei, P.-G., Morales, F., Gueton, O., et al. (2023). Gamma-ray spectroscopy for the characterization of uranium contamination in nuclear decommissioning. *EPJ Web of Conferences*, *288*, 07005. https://doi.org/10.1051/epjconf/202328807005

Salvador, F., Marchais, T., Pérot, B., Allinei, P.-G., Morales, F., Gueton, O., et al. (2024). Low and high-resolution gamma-ray spectroscopy for the characterization of uranium contamination. *Nuclear Instruments and Methods in Physics Research Section A: Accelerators, Spectrometers, Detectors and Associated Equipment*, *1065*, 169549. https://doi.org/10.1016/j.nima.2024.169549

Sasano, M., Hayashi, M., Yanagawa, Y., Kai, M., Nakano, Y., Osawa, Y., et al. (2025). Application of the Deconvolution Method to Alpha-Ray Energy Spectrum to Improve the Performance of a Radiation Airborne Particulate Monitor. *Journal of Radiation Protection and Research*, *50*(s1), S86–S94. https://doi.org/10.14407/jrpr.2023.00444

SPC Doza. (n.d.). *Progress-AR Alpha Radiometer: Technical Specifications and User Documentation* (User Manual). Moscow, Russia: Scientific Production Company Doza. https://www.doza.ru/docs/eng/adt/spect/spectrometry-ar.pdf. Accessed 26 May 2026

Stegnar, P., Shishkov, I., Burkitbayev, M., Tolongutov, B., Yunusov, M., Radyuk, R., & Salbu, B. (2013). Assessment of the radiological impact of gamma and radon dose rates at former U mining sites in Central Asia. *Journal of Environmental Radioactivity*, *123*, 3–13. https://doi.org/10.1016/j.jenvrad.2012.12.005

Tsukatani, T., Toderich, K., & Goldstein, R. I. (2008). *Uranium mine aftermath and Yangiabad Expedition in Uzbekistan* (Discussion Paper No. 647). Kyoto, Japan: Kyoto University, Institute of Economic Research.

Tukhtaev, U., Khasanov, S., Fayzullayev, J., Safarov, A., Togaev, B., & Afsharipour, S. (2024). Determination of natural radionuclides and heavy metal concentrations in the groundwater and adjacent areas of the Kattakurgan reservoir, Uzbekistan. *Radiochimica Acta*, *112*(2), 127–137. https://doi.org/10.1515/ract-2023-0254

UNSCEAR. (2000). *Sources and Effects of Ionizing Radiation: UNSCEAR 2000 Report to the General Assembly, with Scientific Annexes. Volume I: Sources*. New York: United Nations. https://www.unscear.org/unscear/en/publications/2000_1.html

UNSCEAR. (2010). *Sources and Effects of Ionizing Radiation: UNSCEAR 2008 Report to the General Assembly, with Scientific Annexes. Volume I: Sources*. New York: United Nations.

Urunov, I., Allaberganova, G., Muzafarov, A., & Quvvatova, M. (2024). Studying the possibility of applying spectral methods for the analysis of chemical elements and radionuclides. *E3S Web of Conferences*, *525*, 04005. https://doi.org/10.1051/e3sconf/202452504005

WNA. (2026). Uranium in Uzbekistan. World Nuclear Association. https://world-nuclear.org/information-library/country-profiles/countries-t-z/uzbekistan. Accessed 1 July 2026

World Bank Group. (2020). Climatology Data (1991–2020). *Climate Change Knowledge Portal*. World Bank Group. https://climateknowledgeportal.worldbank.org. Accessed 1 July 2026

Yılmazkaya, İ., Altinsoy, N., & Şimşek, V. (2025). Radiologic risk assessment of outdoor gamma dose rate in Çorum province, Turkey. *Journal of Radioanalytical and Nuclear Chemistry*, *334*(9), 6633–6639. https://doi.org/10.1007/s10967-025-10023-3

Zar, J. H. (2010). *Biostatistical Analysis* (5th ed.). Upper Saddle River, NJ, USA: Prentice Hall.